ACS APPLIED MATERIALS & INTERFACES

Letter

www.acsami.org

Efficient Light Harvester Layer Prepared by Solid/Mist Interface Reaction for Perovskite Solar Cells

Xiang Xia,[†] Hongcui Li,[†] Wenyi Wu,[‡] Yanhua Li,[†] Dehou Fei,[†] Chunxiao Gao,*[,‡] and Xizhe Liu*[,†]

[†]Institute of Atomic and Molecular Physics, Jilin Provincial Key Laboratory of Applied Atomic and Molecular Spectroscopy, and [‡]State Key Laboratory for Superhard Materials, Jilin University, Changchun, 130012, China

Supporting Information

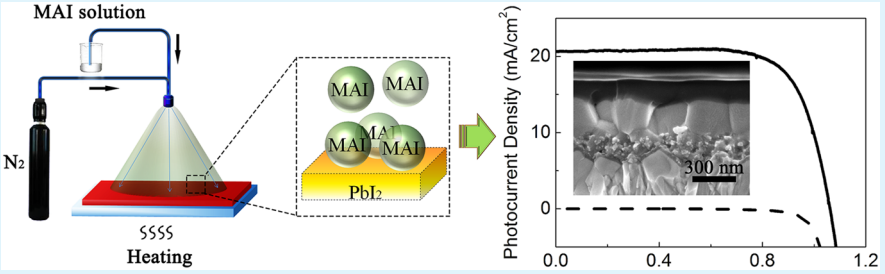

ABSTRACT: A solid/mist reaction method is developed to produce well-crystallized light harvester layers without pinhole defects for perovskite solar cells. The reaction based on mist precursor can be facilely operated with low process temperature. And it can effectively control the volume of CH_3NH_3I solution and the reaction temperature, which affect the quality of perovskite harvester layers and the performance of perovskite solar cells remarkably. Under optimized condition, the efficiencies of devices reach 16.2% with the average efficiency of 14.9%. The solid/mist reaction is also used to fabricate planar junction solar cells and a PCE of 14.9% is obtained.

KEYWORDS: *solar cells, perovskite formation process, morphology-control, low-temperature fabrication, interface reaction, mist*

Hybrid organic/inorganic lead halide, which has a perovskite structure, is a kind of new emerging light harvester materials with excellent photovoltaic performance. This kind of perovskite material is originally developed as soluble semiconductors with high carrier mobility. As it has tunable optical properties, this material is also the effective harvester in perovskite solar cells.[1,2] By using a solid state heterostructure, perovskite solar cells achieve the light to electrical power conversion efficiencies (PCEs) of 9.7% and 10.9% in 2012.[3,4] Further improvement on interface and composition leads to the conversion efficiency of 18−20%,[5,6] which approaches the performance of c-Si solar cells and CIGS solar cells.

$CH_3NH_3PbI_3$ is a wildly investigated perovskite material for the light harvester layers in perovskite solar cells.[7−10] It is found that pinhole-free perovskite films with high crystallization benefit the device performance and its reproducibility.[11−16] Therefore, the fabrication of high-quality perovskite films becomes one of the central topics in perovskite solar cells. $CH_3NH_3PbI_3$ film is usually synthesized by the reaction between lead iodide (PbI_2) and methylammonium iodide (MAI). Although annealing the composite film of these reactants is a direct method for fabricating $CH_3NH_3PbI_3$ films, its uncontrollable morphology degrades the reproducibility of the photovoltaic devices.[3] As improving the morphology of composite films need additional precise control, fabrication methods based on interface reaction are wildly used.[14−22]

Perovskite films can be fabricated by the solid/liquid interface reaction between PbI_2 film and MAI solution.[17,18] This solution-based method is wildly used for its facile operation and low process temperature. However, pinhole defects exist on the perovskite films, which leads to the relatively low average PCE (12.0%) of solar cells.[17] As PbI_2 film is dipped in the MAI solution in this reaction, the direct contact between PbI_2 film and MAI solution limits the precise control of solution volume. The modified method based on two-step spin-coating procedure can produce well crystallized $MAPbI_3$ cuboids, but pinhole defects still exist.[18] The direct contact between PbI_2 film and MAI solution also limits the optimization of reaction temperature, because the temperature affects the solubility of perovskite material in the MAI solution.

Perovskite film can also be fabricated by the reaction at solid/vapor interface. By transporting MAI vapor in inert carrier gas to the reaction interface, efficient perovskite light harvester film can be prepared, and the p-i-n solar cell and p-free solar cell achieve PCEs of 12.1 and 10.6%, respectively.[14−16] Chemical vapor deposition technique is also used for fabricating perovskite film at the solid/vapor interface.[19,20] In this method, PbI_2 film was separated from MAI source. In this way, the separately control on the reaction temperature can be

Received: May 26, 2015
Accepted: July 30, 2015
Published: July 30, 2015

DOI: 10.1021/acsami.5b04563
ACS Appl. Mater. Interfaces 2015, 7, 16907−16912

performed. Comparing with solution-based method, the vapor-based method usually needs a relatively high process temperature, but the reaction is still slow. It implies that solvent plays an essential role on the formation and crystallization of perovskite film at low temperature.

Spray technique can generate mist, which is a different precursor from solution and vapor. As spray is a wildly used technique, interface reaction based on mist precursor can be facilely operated in industry productions. $MAPbI_{3-x}Cl_x$ and $MAPbI_3$ films are prepared by spraying the mixed solution of MAI and lead halides, and corresponding devices achieve the efficiencies of 11.1 and 10.2%, respectively.[23,24] These one-step deposition methods have the problem of redissolving predeposited films by the solution mist.

In this study, two-step method based on solid/mist interface reaction can solve this problem by adopting a separate solvent for MAI, which does not dissolve PbI_2 or $MAPbI_3$. As a modified solution-based method, the solid/mist interface reaction is facilely operated with low process temperature. Instead of direct contact with MAI solution, the MAI microdroplets are transported to the reaction interface by inert carrier gas, which is just like the vapor-based method. In this way, the volume of MAI solution and the reaction temperature can be controlled effectively.

Scheme 1 illustrates the formation process of perovskite film at solid/mist interface. First, the PbI_2 film was heated to the

Scheme 1. (a) Schematic Illustration of Perovskite Film Formation via Solid/Mist Interface Reaction, Photographs of PbI_2 Films (b) before and (c) after the Solid/Mist Reaction

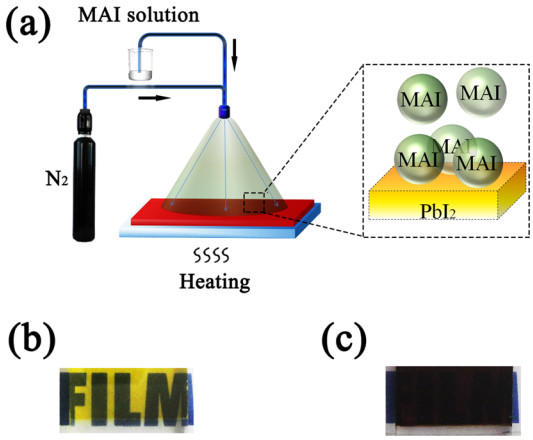

desired temperature on a hot plate. Then, 10 mg/mL MAI in isopropanol solution was nebulized and sprayed on the top of the PbI_2 film by a nitrogen gas atomizing spray nozzle. In this process, the quantity of reactant and the reaction temperature can be facilely controlled by adjusting the sprayed volume of MAI solution and the temperature of hot plate. The photographs of PbI_2 films before and after the solid/mist reaction are shown in Scheme 1b, c, respectively. Details for material preparation and device fabrication can be found in the Supporting Information.

In the solid/mist interface reaction, six $MAPbI_3$ samples are prepared by MAI solutions with different volumes (50, 100, 200, 400, 600, and 1000 μL, respectively), and the reaction temperature is kept at 80 °C. X-ray diffraction (XRD) patterns of these $MAPbI_3$ films are shown in Figure 1a. Meanwhile,

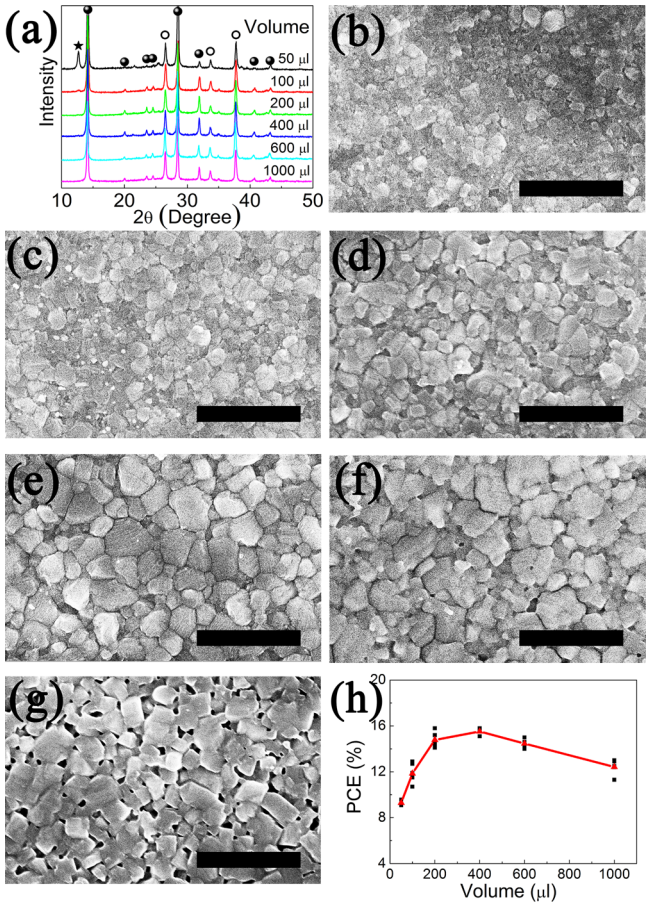

Figure 1. (a) X-ray diffraction (XRD) patterns, (b–g) top-view SEM images, and (h) device efficiency (PCE) of the $MAPbI_3$ films prepared with various volumes of MAI solution. The XRD peaks assigned to $MAPbI_3$, PbI_2, and FTO crystals are marked with solid circles, asterisks and open circles, respectively. For SEM images, MAI solution volumes are (b) 50, (c) 100, (d) 200, (e) 400, (f) 600, and (g) 1000 μL, and the scale bar is 1 μm.

TiO_2/FTO substrate, PbI_2 film, and MAI film are measured as the references (Figure S1). In the XRD patterns of the $MAPbI_3$ films (Figure 1a), a set of strong peaks (marked with solid circle) assigned to $MAPbI_3$ crystal indicate a tetragonal crystal structure of halide perovskite. Furthermore, an extra strong peak at 12.65° exists in the XRD pattern of the $MAPbI_3$ film prepared by 50 μL of MAI solution, which belongs to the residual PbI_2. This indicates that 50 μL of MAI solution is not enough to complete the conversion from PbI_2 to $MAPbI_3$. Moreover, the intensity of the PbI_2 characteristic peak attenuates in the $MAPbI_3$ films prepared by 100 μL of MAI solution, and disappears at 200 μL. All of the $MAPbI_3$ films prepared by 200–1000 μL of MAI solution show the similar characteristic peaks in the XRD patterns. Therefore, 200 μL of MAI solution is enough for the conversion from PbI_2 to $MAPbI_3$. This volume is much lower than that used in solid/liquid reaction.

Scanning electron microscope (SEM) images of the $MAPbI_3$ films prepared with different volumes of MAI solution are shown in Figure 1b–g. As shown in Figure 1b, poorly crystallized $MAPbI_3$ film with nonuniform crystal grain size is prepared by 50 μL of MAI solution. With increasing of MAI solution from 50 to 400 μL, the crystal grains of the $MAPbI_3$ film are grown (Figure 1b–e). Although 200 μL of MAI

DOI: 10.1021/acsami.5b04563
ACS Appl. Mater. Interfaces 2015, 7, 16907–16912

solution is enough for converting PbI_2 to $MAPbI_3$, a further increase in MAI solution to 400 μL can improve the crystallization of $MAPbI_3$ film. Previous reports show that DMF vapor and water vapor can enhance the crystal growth of perovskite light harvester films.[25−27] Although the treatment time is much shorter than that of solvent vapor treatment, the crystal growth in Figure 1b−e implies that solution mist treatment is also an effective technique for improving the crystallization of perovskite films. Comparing with the compact morphology in Figure 1b−e, small pinholes emerge in the $MAPbI_3$ films prepared by 600 μL of MAI solution (Figure 1f). In Figure 1g, the $MAPbI_3$ crystal grains distribute loosely, and holes with the size of 50 nm appear in the film prepared by 1000 μL of MAI solution. It is found that the excessive MAI solution leads to a polyhedral shape of the $MAPbI_3$ crystal grains (Figure 1g), which is just like the crystal grains prepared by the solid/liquid reaction (Figure S2). Therefore, the volume of MAI solution is an important factor for controlling the morphology of $MAPbI_3$ films.

The PCEs of the devices based on these $MAPbI_3$ films are summarized in Figure 1h, and the photovoltaic parameters are summarized in Table S1. For each solution volume, five devices are fabricated. As shown in Figure 1h, the devices fabricated with 50 μL of MAI solution give the lowest average efficiency of 9.3%. The average efficiency increases to 11.9 and 14.8% when MAI solution is increased to 100 and 200 μL, respectively. For the $MAPbI_3$ film prepared with 400 μL of MAI solution, the corresponding devices achieve the highest average efficiency of 15.5%, and its uncertainty is the lowest one among six fabrication conditions. SEM images and XRD patterns show that $MAPbI_3$ crystal grains are grown and residual PbI_2 are decreased by the increment of MAI solution from 50 to 400 μL. As a consequence, the grain boundaries and defects of the $MAPbI_3$ film are reduced, and the lifetime and mobility of charge carriers can be improved.[11,12] As the volume of MAI solution further increases to 600 μL and 1000 μL, the average efficiency reduces to 14.5% and 12.4% respectively. SEM images (Figure 1f and g) show that pinholes emerge in the $MAPbI_3$ film prepared under these conditions. These pinholes can provide the shunt path for leakage current, which leads to the decrease on fill factor and short circuit current density (J_{SC}) (Table S1).[15,28]

The solid/mist interface reaction permits the control of reaction temperature without disturbing the temperature of MAI solution source. Six reaction temperatures (40, 60, 80, 100, 120, and 140 °C, respectively) are applied to study the effect of reaction temperature in the formation of $MAPbI_3$ film. The volume of MAI solution is kept at 400 μL. The XRD patterns of the $MAPbI_3$ films prepared at various reaction temperatures are shown in Figure 2a. At the reaction temperature of 40 °C, XRD pattern of the prepared film gives a diffraction peak at 12.65°, which belongs to unreacted PbI_2. Low reaction temperature leads to low reaction rate between PbI_2 and MAI, which results in the residual PbI_2 existed after the reaction. When reaction temperature increases to the range from 60 to 120 °C, the absence of PbI_2 characteristic peak suggests the complete conversion from PbI_2 to $MAPbI_3$. Furthermore, at high reaction temperatures of 140 °C, PbI_2 characteristic peak reappears, which comes from the thermal decomposition of $MAPbI_3$.

SEM images of the $MAPbI_3$ films prepared at different reaction temperatures are shown in Figure 2b−g. Figure 2b shows the $MAPbI_3$ film prepared at 40 °C, which exhibits poor

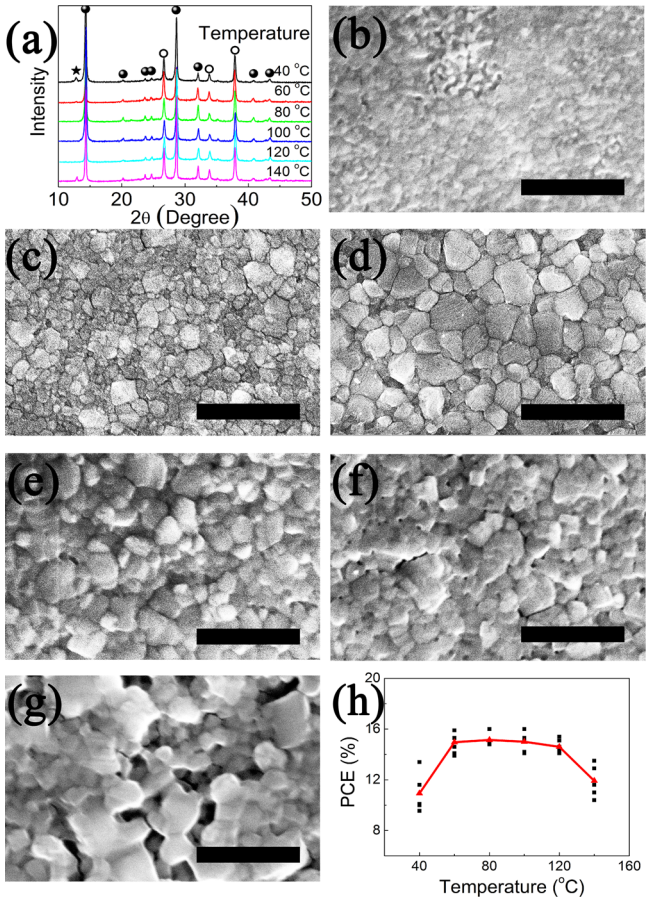

Figure 2. (a) X-ray diffraction (XRD) patterns, (b−g) top-view SEM images, and (h) device efficiency (PCE) of the $MAPbI_3$ films prepared at various reaction temperatures. The XRD peaks assigned to $MAPbI_3$, PbI_2, and FTO crystals are marked with solid circles, asterisks, and open circles, respectively. For SEM images, the reaction temperatures are (b) 40, (c) 60, (d) 80, (e) 100, (f) 120, and (g) 140 °C, the scale bar is 1 μm.

crystallinity. After increasing the reaction temperature to the range from 60 to 100 °C, the prepared $MAPbI_3$ films have compact structure, but perovskite crystal grains are different in size (Figure 2c−e). Large perovskite crystal grains are obtained at high reaction temperature. This result means that the growth rate of perovskite crystal is faster at higher temperature. Some unobvious pinholes appear in the $MAPbI_3$ film prepared at 120 °C (Figure 2f), and further increase of the reaction temperature (140 °C) makes pinholes into obvious holes (Figure 2g). Therefore, reaction temperature not only determines the composition but also the morphology of $MAPbI_3$ films.

The PCEs of the devices based on the $MAPbI_3$ films prepared at different temperature are summarized in Figure 2h, and the photovoltaic parameters are summarized in Table S2. For the reaction temperature of 40 °C, the devices have a relatively low average efficiency of 10.9%. XRD and SEM analysis (Figure 2a, b) indicate that poorly crystallized $MAPbI_3$ film with residual PbI_2 is produced at 40 °C. These structure defects can block the transport of charge carriers and facilitate the recombination process in the device.[11,12] As shown in the above discussion, increasing reaction temperature can improve the crystallization of $MAPbI_3$ films and eliminate residual PbI_2. Highly efficient devices (~15% in PCE) can be fabricated at the reaction temperature between 60 and 120 °C. In the reports of

DOI: 10.1021/acsami.5b04563
ACS Appl. Mater. Interfaces 2015, 7, 16907−16912

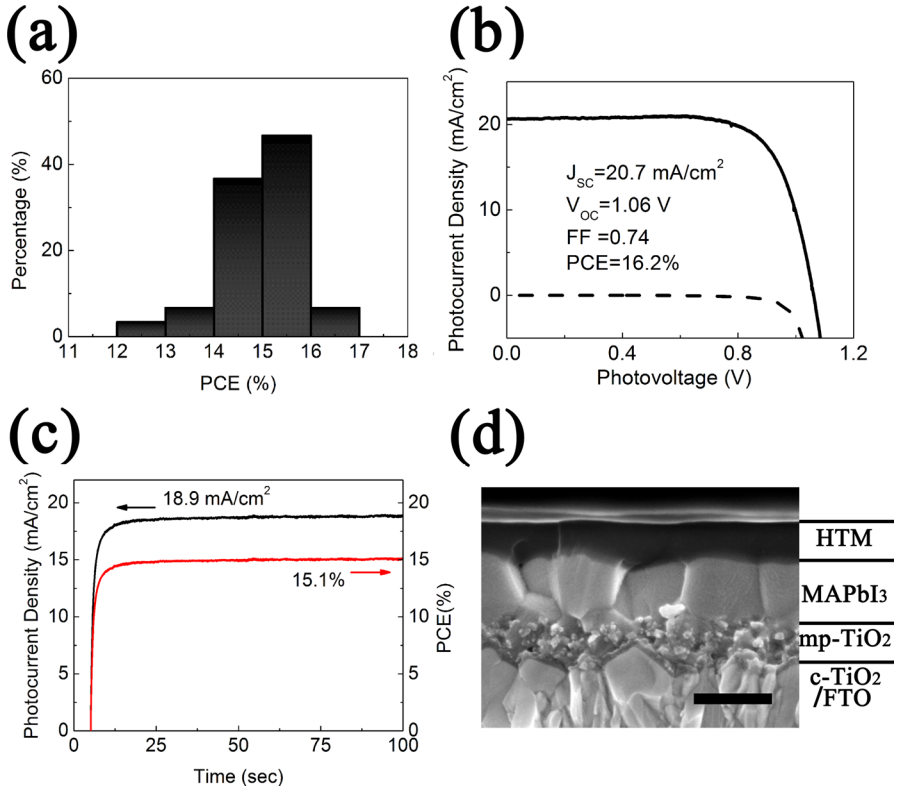

Figure 3. (a) Device performance statistics based on 30 devices, (b) photocurrent density−photovoltage characteristic of the best-performing device (solid line) and the dark *I*−*V* curve (dash line), (c) steady-state current measured at a forward bias of 0.80 V and stabilized power output, (d) cross-sectional SEM image of the device, mp-TiO_2 represents the mesoporous TiO_2 layer penetrated with $MAPbI_3$, c-TiO_2 represents the compact TiO_2 layer, the scale bar is 300 nm.

solid/vapor methods, the reactions are usually conducted at 120−150 °C for 1−2 h.[14−16] On the contrary, solid/mist reaction can be performed at 60 °C, and the reaction can complete in 2 min. Therefore, solid/mist method is a facile low temperature method with high throughput. After further increasing the reaction temperature to 140 °C, PCEs of the devices remarkable decrease to 11.9%. At high reaction temperature, the $MAPbI_3$ film is partially decomposed (Figure 2a) and pinhole defects (Figure 2g) exist in the film. The damaged light harvester film leads to an obvious decrease in J_{SC}. And the porous nature of the high temperature prepared $MAPbI_3$ film increases the leakage current between TiO_2 and hole conductor.[15,28]

The solid/mist reaction method can produce high-quality $MAPbI_3$ films by the facile control of reaction conditions. We fabricate a series of 30 devices under the optimized condition of 400 μL MAI solution and 80 °C. The statistics of PCEs based on the 30 devices is shown in Figure 3a. More than 90% of the devices achieve an efficiency of above 14%. It indicates that this solid/mist interface reaction method has excellent reproducibility and high performance. The photocurrent density-photovoltage characteristic of the best-performing device is depicted in Figure 3b. The device exhibits outstanding power conversion efficiency of 16.2%, with 20.7 mA/cm^2 in J_{SC}, 1.06 V in open circuit voltage V_{OC} and 0.74 in fill factor (FF). We also records the photocurrent of a device held at a forward bias of 0.80 V as the function of time to gain some understanding of the stabilized power output under working conditions (Figure 3c). The photocurrent stabilizes within seconds to approximately 18.9 mA/cm^2, yielding a stabilized power conversion efficiency of 15.1%, measured after 100 s. This indicates that the devices have good working-stability. Furthermore, this stabilized efficiency is closer to the efficiency measured via reverse scan (15.8%) than that via forward scan (13.6%) (Figure S3). It implies that reverse scan can provide a relatively accurate representation of the photovoltaic performance for this kind of devices. The cross-sectional SEM image of a device is shown in Figure 3d. Highly crystallized $MAPbI_3$ capping layer without pinhole defects covers on mesoporous TiO_2 layer. The $MAPbI_3$ grains in the capping layer are so large that a single grain can connect the TiO_2 layer and the hole conductor layer. The elimination of grain boundaries can alleviate carrier recombination and facilitate charge transport in the $MAPbI_3$ layer.[11,12]

Furthermore, planar junction perovskite solar cells are also fabricated using this solid/mist interface reaction (Figure S4). Planar junction device is attractive for its simple device structure, but pinhole free perovskite film with high crystallization is necessary to prevent the leakage current and enhance the carrier diffusion.[28−32] The excellent efficiency of 14.9% confirms the availability of the solid/mist method.

In summary, we develop a solid/mist interface reaction method to fabricate $CH_3NH_3PbI_3$ light harvester film for perovskite solar cells. In this method, high-quality $CH_3NH_3PbI_3$ films can be prepared at low temperature, and reaction conditions can be facilely controlled. Detail studies reveal that the volume of CH_3NH_3I solution and the reaction temperature control not only the extent of reaction but also the morphology and crystallization of the $CH_3NH_3PbI_3$ film. Under optimized conditions, pinhole-free $CH_3NH_3PbI_3$ films with high crystallization can be obtained, and the PCEs of corresponding devices reach 16.2% with the average efficiency

DOI: 10.1021/acsami.5b04563
ACS Appl. Mater. Interfaces 2015, 7, 16907−16912

of 14.9%. This method is also effective for fabricating planar junction perovskite solar cells. This reaction based on mist precursor is enlargeable with high throughput, which is suitable for industrial application. We think that this solid/mist reaction can be a general method for fabricating perovskite light harvester films, and it also has potential in other compound films.

■ ASSOCIATED CONTENT

Supporting Information

The Supporting Information is available free of charge on the ACS Publications website at DOI: 10.1021/acsami.5b04563.

Experimental details, device photovoltaic parameters, XRD patterns for references, SEM images for references, *I*−*V* characteristic via different scanning directions, *I*−*V* characteristic of the planar junction device, the effect of MAI solution concentration, comparison of Ag and Au top electrode, IPCE spectrum (PDF)

■ AUTHOR INFORMATION

Corresponding Author

*E-mail: liu_xizhe@jlu.edu.cn.

Notes

The authors declare no competing financial interest.

■ ACKNOWLEDGMENTS

This work was partially supported by National Science Foundation of China (Grants 51273079, 11374121), National Basic Research Program of China (Grant 2011CB808204), the Science Development Program of JiLin Province (Grant 20150519021JH), and the Fundamental Research Funds for Central Universities at Jilin University.

■ REFERENCES

(1) Kojima, A.; Teshima, K.; Shirai, Y.; Miyasaka, T. Organometal Halide Perovskites as Visible-Light Sensitizers for Photovoltaic Cells. *J. Am. Chem. Soc.* **2009**, *131*, 6050−6051.

(2) Im, J.; Lee, C.; Lee, J.; Park, S.; Park, N. 6.5% Efficient Perovskite Quantum-Dot-Sensitized Solar Cell. *Nanoscale* **2011**, *3*, 4088−4093.

(3) Kim, H.; Lee, C.; Im, J.; Lee, K.; Moehl, T.; Marchioro, A.; Moon, S.; Humphry-Baker, R.; Yum, J.; Moser, J.; Grätzel, M.; Park, N. Lead Iodide Perovskite Sensitized All-Solid-State Submicron Thin Film Mesoscopic Solar Cell with Efficiency Exceeding 9%. *Sci. Rep.* **2012**, *2*, 591.

(4) Lee, M.; Teuscher, J.; Miyasaka, T.; Murakami, T.; Snaith, H. Efficient Hybrid Solar Cells Based on Meso-Superstructured Organometal Halide Perovskites. *Science* **2012**, *338*, 643−647.

(5) Zhou, H.; Chen, Q.; Li, G.; Luo, S.; Song, T.; Duan, H. S.; Hong, Z.; You, J.; Liu, Y.; Yang, Y. Interface Engineering of Highly Efficient Perovskite Solar Cells. *Science* **2014**, *345*, 542−546.

(6) Jeon, N.; Noh, J.; Yang, W.; Kim, Y.; Ryu, S.; Seo, J.; Seok, S. Compositional Engineering of Perovskite Materials for High-Performance Solar Cells. *Nature* **2015**, *517*, 476−480.

(7) Yin, X.; Guo, Y.; Xue, Z.; Xu, P.; He, M.; Liu, B. Performance Enhancement of Perovskite-Sensitized Mesoscopic Solar Cells Using Nb-Doped TiO_2 Compact Layer. *Nano Res.* **2015**, *8*, 1997−2003.

(8) Etgar, L.; Gao, P.; Xue, Z.; Peng, Q.; Chandiran, A.; Liu, B.; Nazeeruddin, M. K.; Grätzel, M. Mesoscopic $CH_3NH_3PbI_3/TiO_2$ Heterojunction Solar Cells. *J. Am. Chem. Soc.* **2012**, *134*, 17396−17399.

(9) Hu, Q.; Wu, J.; Jiang, C.; Liu, T.; Que, X.; Zhu, R.; Gong, Q. Engineering of Electron-Selective Contact for Perovskite Solar Cells with Efficiency Exceeding 15%. *ACS Nano* **2014**, *8*, 10161−10167.

(10) Xiao, J.; Shi, J.; Liu, H.; Xu, Y.; Lv, S.; Luo, Y.; Li, D.; Meng, Q.; Li, Y. Efficient $CH_3NH_3PbI_3$ Perovskite Solar Cells Based on Graphdiyne(GD)-Modified P3HT Hole-Transporting Material. *Adv. Energy Mater.* **2015**, *5*, 1401943.

(11) Nie, W.; Tsai, H.; Asadpour, R.; Blancon, J.; Neukirch, A.; Gupta, G.; Crochet, J.; Chhowalla, M.; Tretiak, S.; Alam, M.; Wang, H.; Mohite, A. High-Efficiency Solution-Processed Perovskite Solar Cells with Millimeter-Scale Grains. *Science* **2015**, *347*, 522−525.

(12) deQuilettes, D.; Vorpahl, S.; Stranks, S.; Nagaoka, H.; Eperon, G.; Ziffer, M. E.; Snaith, H.; Ginger, D. Solar cells. Impact of Microstructure on Local Carrier Lifetime in Perovskite Solar Cells. *Science* **2015**, *348*, 683−686.

(13) Heo, J.; Song, D.; Han, H.; Kim, S.; Kim, J.; Kim, D.; Shin, H.; Ahn, T.; Wolf, C.; Lee, T.; Im, S. Planar $CH_3NH_3PbI_3$ Perovskite Solar Cells with Constant 17.2% Average Power Conversion Efficiency Irrespective of the Scan Rate. *Adv. Mater.* **2015**, *27*, 3424−3430.

(14) Chen, Q.; Zhou, H.; Hong, Z.; Luo, S.; Duan, H. S.; Wang, H. H.; Liu, Y. S.; Li, G.; Yang, Y. Planar Heterojunction Perovskite Solar Cells via Vapor-Assisted Solution Process. *J. Am. Chem. Soc.* **2014**, *136*, 622−625.

(15) Hao, F.; Stoumpos, C. C.; Liu, Z.; Chang, R.; Kanatzidis, M. Controllable Perovskite Crystallization at a Gas-Solid Interface for Hole Conductor-Free Solar Cells with Steady Power Conversion Efficiency over 10%. *J. Am. Chem. Soc.* **2014**, *136*, 16411−16419.

(16) Li, Y.; Cooper, J.; Buonsanti, R.; Giannini, C.; Liu, Y.; Toma, F.; Sharp, I. Fabrication of Planar Heterojunction Perovskite Solar Cells by Controlled Low-Pressure Vapor Annealing. *J. Phys. Chem. Lett.* **2015**, *6*, 493−499.

(17) Burschka, J.; Pellet, N.; Moon, S.; Humphry-Baker, R.; Gao, P.; Nazeeruddin, M.; Grätzel, M. Sequential Deposition as a Route to High-Performance Perovskite-Sensitized Solar Cells. *Nature* **2013**, *499*, 316−319.

(18) Im, J.; Jang, I.; Pellet, N.; Grätzel, M.; Park, N. Growth of $CH_3NH_3PbI_3$ Cuboids with Controlled Size for High-Efficiency Perovskite Solar Cells. *Nat. Nanotechnol.* **2014**, *9*, 927−932.

(19) Leyden, M.; Ono, L.; Raga, S.; Kato, Y.; Wang, S.; Qi, Y. High Performance Perovskite Solar Cells by Hybrid Chemical Vapor Deposition. *J. Mater. Chem. A* **2014**, *2*, 18742−18745.

(20) Luo, P.; Liu, Z.; Xia, W.; Yuan, C.; Cheng, J.; Lu, Y. Uniform, Stable, and Efficient Planar-Heterojunction Perovskite Solar Cells by Facile Low-Pressure Chemical Vapor Deposition under Fully Open-Air Conditions. *ACS Appl. Mater. Interfaces* **2015**, *7*, 2708−2714.

(21) Xu, Y.; Zhu, L.; Shi, J.; Lv, S.; Xu, X.; Xiao, J.; Dong, J.; Wu, H.; Luo, Y.; Li, D.; Meng, Q. Efficient Hybrid Mesoscopic Solar Cells with Morphology-Controlled $CH_3NH_3PbI_{3-x}Cl_x$ Derived from Two-Step Spin Coating Method. *ACS Appl. Mater. Interfaces* **2015**, *7*, 2242−2248.

(22) Shi, J.; Luo, Y.; Wei, H.; Luo, J.; Dong, J.; Lv, S.; Xiao, J.; Xu, Y.; Zhu, L.; Xu, X.; Wu, H.; Li, D.; Meng, Q. Modified Two-Step Deposition Method for High-Efficiency $TiO_2/CH_3NH_3PbI_3$ Heterojunction Solar Cells. *ACS Appl. Mater. Interfaces* **2014**, *6*, 9711−9718.

(23) Barrows, A.; Pearson, A.; Kwak, C.; Dunbar, A.; Buckley, A.; Lidzey, D. Efficient Planar Heterojunction Mixed-halide Perovskite Solar Cells Deposited via Spray Deposition. *Energy Environ. Sci.* **2014**, *7*, 2944−2950.

(24) Ramesh, M.; Boopathi, K.; Huang, T.; Huang, Y.; Tsao, C.; Chu, C. Using an Airbrush Pen for Layer-by-Layer Growth of Continuous Perovskite Thin Films for Hybrid Solar Cells. *ACS Appl. Mater. Interfaces* **2015**, *7*, 2359−2366.

(25) Xiao, Z.; Dong, Q.; Bi, C.; Shao, Y.; Yuan, Y.; Huang, J. Solvent Annealing of Perovskite-Induced Crystal Growth for Photovoltaic-Device Efficiency Enhancement. *Adv. Mater.* **2014**, *26*, 6503−6509.

(26) You, J.; Yang, Y.; Hong, Z.; Song, T. B.; Meng, L.; Liu, Y.; Jiang, C.; Zhou, H.; Chang, W. H.; Li, G.; Yang, Y. Moisture Assisted Perovskite Film Growth for High Performance Solar Cells. *Appl. Phys. Lett.* **2014**, *105*, 183902.

(27) Zhu, W.; Yu, T.; Li, F.; Bao, C.; Gao, H.; Li, Y.; Yang, J.; Fu, G.; Zhou, X.; Zou, Z. A Facile, Solvent Vapor-Fumigation-Induced, Self-

DOI: 10.1021/acsami.5b04563
ACS Appl. Mater. Interfaces 2015, 7, 16907−16912

Repair Recrystallization of $CH_3NH_3PbI_3$ Films for High-Performance Perovskite Solar Cells. *Nanoscale* **2015**, *7*, 5427−5434.
(28) Eperon, G.; Burlakov, V.; Docampo, P.; Goriely, A.; Snaith, H. Morphological Control for High Performance, Solution-Processed Planar Heterojunction Perovskite Solar Cells. *Adv. Funct. Mater.* **2014**, *24*, 151−157.
(29) Jeon, N.; Noh, J.; Kim, Y.; Yang, W.; Ryu, S.; Seok, S. Solvent Engineering for High-Performance Inorganic-Organic Hybrid Perovskite Solar Cells. *Nat. Mater.* **2014**, *13*, 897−903.
(30) Wu, Y.; Islam, A.; Yang, X.; Qin, C.; Liu, J.; Zhang, K.; Peng, W.; Han, L. Retarding the Crystallization of PbI_2 for Highly Reproducible Planar-Structured Perovskite Solar Cells via Sequential Deposition. *Energy Environ. Sci.* **2014**, *7*, 2934−2938.
(31) Xiao, M.; Huang, F.; Huang, W.; Dkhissi, Y.; Zhu, Y.; Etheridge, J.; Weale, A.; Bach, U.; Cheng, Y.; Spiccia, L. A Fast Deposition-Crystallization Procedure for Highly Efficient Lead Iodide Perovskite Thin-Film Solar Cells. *Angew. Chem., Int. Ed.* **2014**, *53*, 9898−9903.
(32) Zhang, W.; Saliba, M.; Moore, D.; Pathak, S.; Horantner, M.; Stergiopoulos, T.; Stranks, S.; Eperon, G.; Alexander-Webber, J.; Abate, A.; Sadhanala, A.; Yao, S.; Chen, Y.; Friend, R.; Estroff, L.; Wiesner, U.; Snaith, H. Ultrasmooth Organic-Inorganic Perovskite Thin-Film Formation and Crystallization for Efficient Planar Heterojunction Solar Cells. *Nat. Commun.* **2015**, *6*, 6142.

DOI: 10.1021/acsami.5b04563
ACS Appl. Mater. Interfaces 2015, 7, 16907−16912